Track Reconstruction with the Silicon Strip Tracker of the Proton CT Phase 2 Scanner

A. Zatserklyaniy, R. P. Johnson, *Member, IEEE*, S. Macafee, T. Plautz, H. Sadrozinski, *Senior Member, IEEE*, V. Bashkirov, F. Hurley, R. Schulte, N. Vence, V. Giacometti

***Abstract*–We present algorithms for the proton track reconstruction for the Phase II proton CT scanner designed and built by the pCT collaboration. The entrance and exit telescopes of the scanner consist of four planes of silicon sensors with horizontal and vertical strips for proton track reconstruction. The goal of the track reconstruction is to allow usage of sub-millimeter voxels for subsequent image reconstruction. A dedicated algorithm was developed that recovers protons that traversed the dead areas at sensor joints and the dead or masked strips. The track reconstruction was tested on the data collected with 200 MeV protons from the proton synchrotron of the Loma Linda University Medical Center. Test results show that the reconstruction accuracy is close to the geometric limit of the strip sensors and multiple Coulomb scattering of the protons in air, sensors and scanning object.**

I. Introduction

PROTON Computed Tomography is capable of providing more accurate data on the Relative to the water Stopping Power (RSP) for the proton radiation therapy planning than a conversion from the Hounsfield data obtained with the X-ray Computed Tomography. In addition, the high registration efficiency of the proton scanner makes proton imaging a low-dose modality [1].

II. Phase II Pre-Clinical pCT Scanner

The Phase II pCT scanner [2] advances the Phase I prototype [3] in a number of ways. The current Phase II prototype features a high rate capable data acquisition system (1 MHz event readout rate has been achieved) and has a new fast Energy detector made out of plastic scintillator.

The tracking part of the scanner is comprised of silicon strip detectors 88x88 mm. Each plane for measuring the vertical and horizontal coordinates consists of four detectors. The pitch size of 228 μm provides a spatial resolution of 70 μm. The extra material on the edges was removed with "slim-edge" technology [4]. Nevertheless there are narrow gaps of dead areas between the detectors. The cassettes were designed with horizontal offsets which prevents a "good" proton to pass through more than one gap in a telescope. Because the hit efficiency of the silicon detectors is 99.9%, an absence of the hit in the layer most likely associated with proton hitting the dead area. If a line drawn from a known beam spot position and existing hit in the neighboring layer passes through the known gap region we can reasonably assume that the hit was missed because the proton passed through the gap.

The known beam spot position helps recover the missing hit in the front telescope with high accuracy and with some loss of accuracy for the rear telescope.

III. Track Reconstruction Features

There are a few very important tracker features for the track reconstruction point of view. Low noise occupancy combined with low expected hit multiplicity (Fig. 1) places a small time penalty on the use of combinatorial algorithms. We build track candidates using all possible combinations of hits, separately for the front and rear telescopes.

An absence of redundant layers prevents fits of the tracks with straight lines. Essentially, all tracks are two-hit straight-line segments. If a proton went through the narrow gap of the dead material between the detectors, the position of the missing hit would need to be recovered.

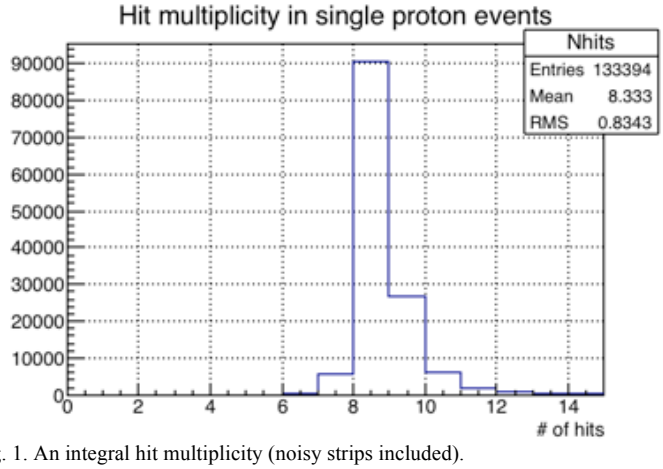

Fig. 1. An integral hit multiplicity (noisy strips included).

The algorithm should take into consideration a significant effect of multiple Coulomb scattering of protons in the energy range of interest.

The Energy detector has no lateral segmentation; that limits the number of useful tracks to one per event.

Manuscript received November 30, 2014. (Write the date on which you submitted your paper for review.) This work was supported in part by the National Institute of Biomedical Imaging and Bioengineering (NIBIB) and the NSF, award Number R01EB013118.

A. Zatserklyaniy, R. P. Johnson, S. Macafee, T. Plautz, and H. F.-W. Sadrozinski, are with the Santa Cruz Institute for Particle Physics and Physics Department, University of California at Santa Cruz, Santa Cruz, CA 95064 (e-mail: zatserkl@ucsc.edu, rjohnson@ucsc.edu, tiaplautz@gmail.com, hartmut@ucsc.edu).

V. Bashkirov, R. F. Hurley, R. Schulte, and N. Vence are with the Division of Radiation Research, Loma Linda University, Loma Linda, CA 92354 (e-mail: vbashkirov@llu.edu, ford.hurley@gmail.com, rschulte@llu.edu, nvence@llu.edu)

V. Giacometti is with the Centre for Medical Radiation Physics, University of Wollongong, Wollongong, NSW, Australia (e-mail: valentina8giacometti@gmail.com).

IV. Coordinate System

Fig. 2 shows the coordinate system. We use a VTU coordinate system where the U-axis is directed along the proton beam, the V-axis is going vertically and T-axis horizontally from the particle eye view.

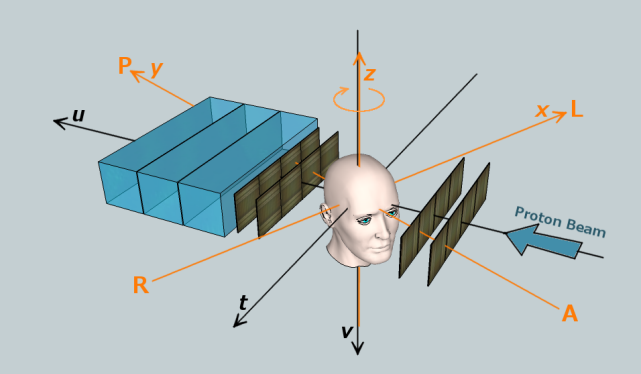

Fig. 2. Coordinate system.

V. Track Reconstruction Algorithm

We describe a 2D track in the front or rear telescope with a straight line in the parametric form. The parameters are an anchor point in the plane U = 0 and two directional cosines. We match pairs of 2D tracks from the front and rear telescopes in the V- and T-plane separately to form 2D "supertracks". To find a projection of the 2D supertrack to the given plane we use a track from the back telescope for the positive hemisphere, and the front telescope track for the negative. Finally the VT-pairs of the 2D supertracks form a 3D supertrack.

At the first stage, we build 2D tracks for all combinations of hits, separately for the front and rear telescope.

On the second stage we match the 2D tracks from the front and rear telescopes based on the distance between the projection of the tracks in the plane U = 0 (the middle of the scanner). Only track pairs with the distance less than 10 mm are considered. This value corresponds to 12.5 standard deviations of the distance distribution when there is no material between the telescopes (the left plot on Fig. 3) or 3.6 standard deviations in presence of a polystyrene block of 204 mm between the telescopes (the right plot on Fig. 3).

At the next stage we build 3D supertracks from T- and V-supertracks. From the readout point of view the V-sensor (vertical coordinate) consist of two horizontal halves. This fact is used to match T-plane tracks with V-plane tracks from the correct half.

The list of the 3D supertracks is a subject of a number of filters that examine the angle between the tracks in the supertrack, distance, orientation with respect to the beam spot position, etc.

At the final stage we apply corrections for the offsets and tilts of the individual detectors. The corrections only change the line parameters, leaving the actual hit values intact, simplifying the data analysis.

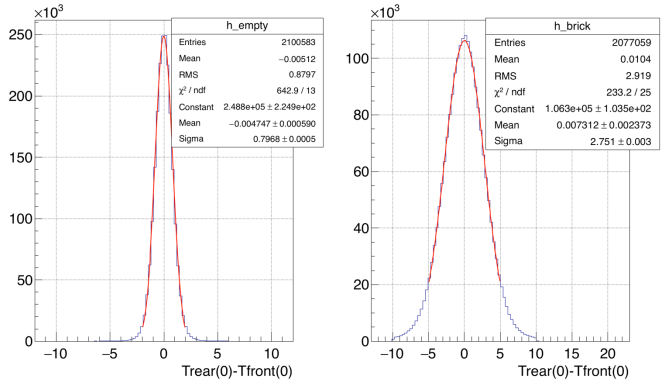

Fig. 3. Distance between track projections into plane u=0 from the front and rear telescopes. Left: σ = 0.80 mm for no material between the telescopes. Right: σ = 2.75 for polystyrene block of 204 mm.

VI. Recovery of the Missing Hits

There are narrow gaps (dead areas) between the silicon detectors in the assembly. When proton passed through these gaps, an absence of a hit prevents a reconstruction of the event with the standard algorithm. Therefore, in case no supertracks were reconstructed, the hit recovery algorithm is launched. The hit recovery algorithm utilizes knowledge of the position of the beam spot at the flange of the accelerator beam pipe and positions of the gaps. In case the projected track from the beam spot to the existing hit in the neighboring layer passes the gap within the limits, an artificial hit will be placed in the gap position. Placing the hit into the center of the gap provides a good enough resolution to use voxels with a size of 0.5 mm. For the front telescope, a weighted average of the track projection and gap center can be used.

Fig. 4 shows a VT scatter plot in the gap region of layer 0. Normal hits are colored red. There is a gap from 2 to 2.6 mm between the T-detectors. The gap around T = 1 mm is a gap between the V-sensors in the same layer. Recovered T-hits are colored green; recovered V-hits are colored blue.

This procedure is straightforward for the front telescope, but also works for the rear telescope because of the high rejection power of the track matching.

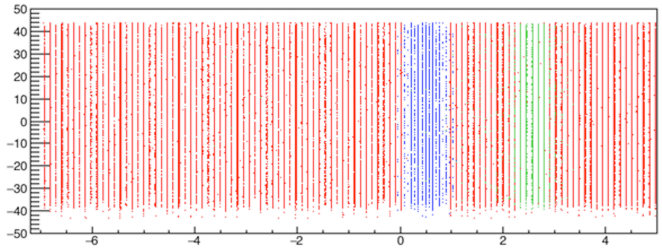

Fig. 4. Scatter plot (V vs T, mm) of the Layer 0 hits. Red: normal hits. Green: recovered missing hits for the t-gap at the T = 2.6 mm, blue: recovered hits for the v-gap at the T = 0.5 mm.

To estimate the hit recovery performance we created an artificial gap and compared the difference between the reconstructed and real positions of the hit. The hit recovery accuracy, σ = 168 μm was better for the front telescope because of better utilization of the beam spot position. The hit reconstruction accuracy for the rear telescope, σ = 290 μm was close to the flat distribution over the gap width.

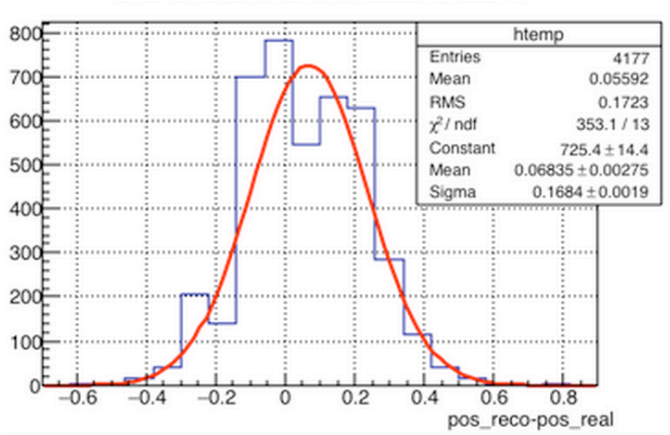

Fig. 5. A difference between the reconstructed and real hit positions for the front telescope.

VII. Tracking Efficiency

To test the track reconstruction efficiency we selected single proton events that had a proper response of the Energy detector and presence of at least one hit in both the T and V sensors in the central part of the front telescope. In absence of a phantom on the rotational stage the track reconstruction efficiency was above 99% for events with 8, 9 and 10. The efficiency of recovering one missing hit was 87% (Fig. 6). Presence of a 204 mm thick polystyrene block decreased the reconstruction efficiency to 96% for events with 8 through 10 hits. The efficiency of recovering of one missing hit was lowered to 85%.

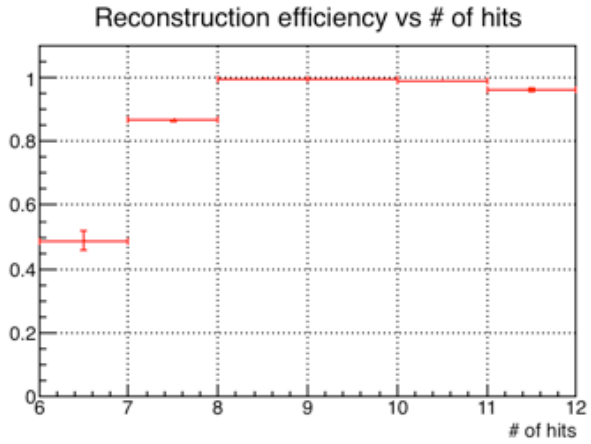

Fig. 6. The reconstruction efficiency (no material between the telescopes).

Fig. 7 shows a profile of the beam spot at the flange of the accelerator beam pipe. The width of the distribution, $\sigma = 13.9$ mm is consistent with the track direction uncertainty and the effects of multiple Coulomb scattering in the 3 m of air and 0.8 mm of silicon added in quadrature.

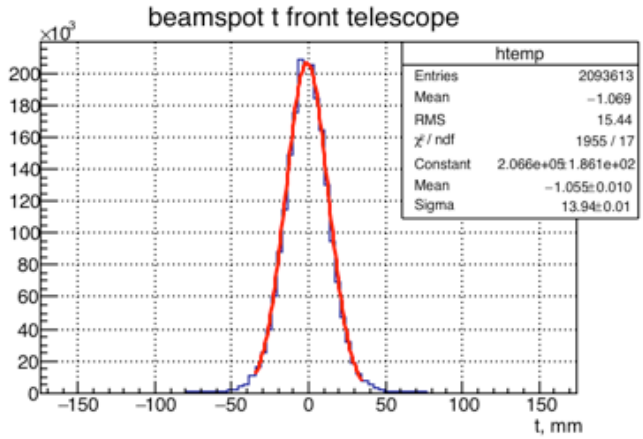

Fig. 7. T-profile of the beam spot.

VIII. Image Reconstruction Results

Fig. 8 shows a reconstructed image of the CATPHAN 404 sensitometry phantom measured with 200 MeV protons.

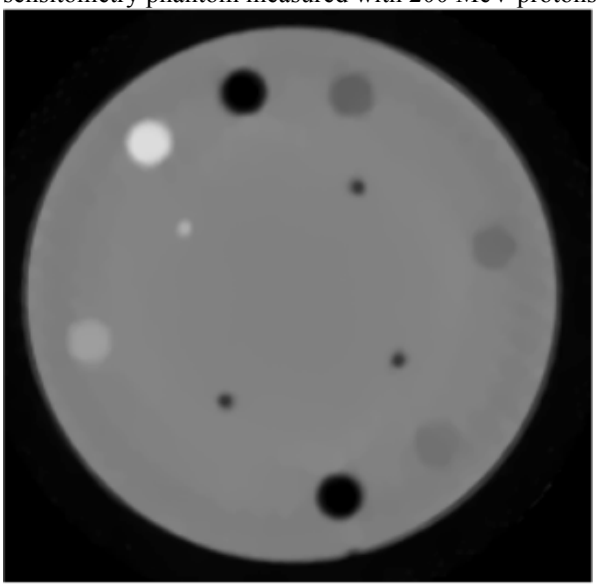

Fig. 8. Reconstructed image of the CATPHAN 404 phantom.

The phantom contains inserts of different density. The image was reconstructed with the Filtered Back Projection method and improved by the iterated algebraic technique. The Most Likely Path formalism [5] was employed for the reconstruction. In total, 75.3M proton histories were used for this image. The angular range was 0 to 356 degree with a step of 4 degrees. Fig. 9 shows a good agreement of reconstructed RSPs of the inserts with actual ones.

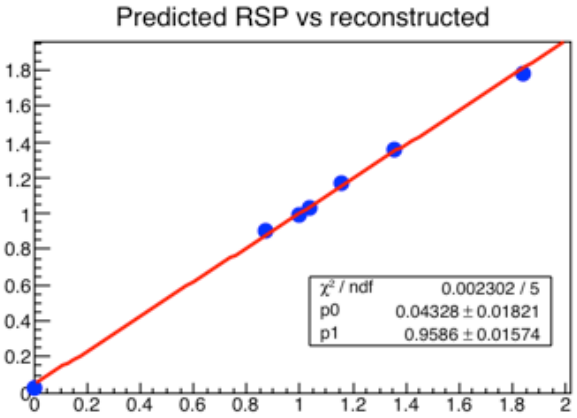

Fig. 9. The reconstructed Relative Stopping Power vs the actual one for the inserts of the Sensitom phantom.

IX. Summary

The track reconstruction algorithm for the Phase II Pre-Clinical Head Scanner provides a track reconstruction efficiency between 96-99% and the recovery of missing hits in the gaps between detectors. The alignment corrections include offsets and tilts. The algorithm takes ¼ of the total time for event processing (the rest is used by read/write operations).

References

[1] R. Schulte, et al., "Conceptual design of a proton Computed Tomography system for applications in proton radiation therapy." *IEEE Trans. Nucl. Sci.* vol. 51, no. 3, June 2004.

[2] H. F.-W. Sadrozinski, *et al.,* "Detector Development for Proton Computed Tomography (pCT)," 2011 IEEE Nuclear Science Symposium Conf. Record, pp. 4457 ‒4461, Oct. 2011.

[3] H.F.-W. Sadrozinski, *et al.,* "Development of a Head Scanner for Proton CT," Nucl. Instr. Meth. A, vol. 699, pp. 205 ‒210, 2013.

[4] M. Christophersen, V. Fadeyev, B.F. Philips, H.F.-W. Sadrosinski, C. Parker, S. Ely, J.G. Wright, Alumina and silicon oxide/nitride sidewall passivation for P- and N-type sensors, Nucl. Instrt. Methods, A699 (2013), pp. 14-17.

[5] D. C. Williams, "The most likely path of an energetic charged particle through a uniform medium". Phys. Med. Biol. 49 (2004) 2899–2911.